Journal of Materials Chemistry A

ARTICLE

Toughening of Y-doped $BaZrO_3$ proton conducting electrolytes by hydration

Received 00th January 20xx,
Accepted 00th January 20xx

DOI: 10.1039/x0xx00000x

www.rsc.org/

Rokas Sažinas,[a] Mari-Ann Einarsrud[a] and Tor Grande[a]

In $BaZr_{1-x}Y_xO_{3-x/2}$ (BZY), the state-of-the-art oxide proton conductors, the proton conductivity is facilitated by hydration of oxygen vacancies. Hydration induces lattice expansion, which may induce stress and thereby potentially reduce the mechanical integrity of fuel cells. Here, we report on the effect of hydration/dehydration on the mechanical properties of dense BZY-materials sintered by two different methods. The chemical expansion due to hydration was determined by X-ray diffraction, and the normalized chemical strain was calculated by combining these data with thermogravimetry. The mechanical properties were investigated by Vickers-micro indentation technique. Hydration was demonstrated to enhance the fracture toughness of the materials with the change in fracture mode from intergranular to transgranular mechanism. We demonstrate that hydration/dehydration process is reversible and discuss the present findings with respect to long-term stability of electrochemical devices based on $BaZrO_3$.

1 Introduction

High fuel utilization and potentially lower operation temperatures have made protonic ceramic fuel cells (PCFC) an attractive alternative to conventional solid oxide fuel cells.[1-7] This potential has resulted in tremendous interest in proton conducting oxide electrolytes with potential high efficiencies at intermediate temperatures (450–700 °C).[6-10] The state of the art proton conducting oxide materials are $BaZr_{1-x}Y_xO_{3-x/2}$ (BZY)[1-6, 9-12] and $BaCe_{1-x}Y_xO_{3-x/2}$ (BCY).[9, 10, 13-15] One of the main challenges with these materials is the instability of the materials in CO_2 containing atmosphere, particularly BCY. Although BZY is thermodynamically more stable than BCY, investigations have demonstrated that BZY may be affected by the reaction with CO_2.[16-19]

The reaction with steam (hydration) is also of paramount importance. Proton conduction in BZY is realized by hydration of oxygen vacancies introduced by acceptor doping (Y).[9, 10] The proton concentration is controlled by the degree of hydration.[9, 10] Both the acceptor doping and the hydration of the oxygen vacancies trigger volume changes of the perovskite lattice. [9, 10, 20] A considerable volume expansion due to hydration was pointed out by Kreuer.[9] Several recent studies have confirmed that hydration of $BaZr_{1-x}Y_xO_{3-x/2}$ results in a volume expansion of the BZY lattice.[21, 22] A detailed description on the phenomenology of chemical expansion due to hydration for BCY/BZY was proposed and a review of available volumetric data on hydration of oxide materials was provided.[22, 23] Chemical expansion due to hydration is generic for any proton-conducting oxide and is perceived to induce strain in the material.[22, 23] The transient strain due to hydration will induce stress, which might cause microcracking of the dense electrolyte in a PCFC.

To assess the chemically induced stress due to hydration, knowledge of the mechanical performance of proton-conducting ceramics in humid atmosphere is essential. As a result, in this study we report on the effect of hydration/dehydration of $BaZr_{1-x}Y_xO_{3-x/2}$ (x = 0.1 and 0.2) and $BaCe_{0.2}Zr_{0.7}Y_{0.1}O_{2.95}$ ceramics on mechanical stability based on recently introduced Vickers-micro indentation technique.[19] The surfaces and the changes in the lattice were monitored by electron microscopy and X-ray diffraction. The degree of hydration was measured by thermogravimetry, and chemical expansion due to hydration was determined by combination with the diffraction data. A particular attention was given to the thermal history, chemical composition and the grain size of the ceramics. An evident toughening of the ceramics due to hydration at temperatures 450–650 °C was demonstrated, and the consequences for mechanical performance of $BaZrO_3$-based electrolytes are discussed.

2 Experimental

2.1 Sample preparation

Fine ceramic powders with composition $BaZr_{1-x}Y_xO_{3-x/2}$ (x = 0.1 and 0.2), denoted as BZY10 and BZY20, respectively and $BaCe_{0.2}Zr_{0.7}Y_{0.1}O_{2.95}$ (BCZY27) used in this study were prepared by spray pyrolysis of aqueous nitrate solutions (CerPoTech AS, Trondheim, Norway). The as-prepared powders were calcined at 950 °C for 12 h, ball milled in 2-propanol for 72 h, dried at 120 °C and sieved (100 Mesh). Green bodies were made by uniaxial pressing at 100 MPa followed by cold isostatic pressing (CIP) at 200 MPa. Dense ceramics were prepared by conventional sintering (procedure I) and sintering with

[a] Department of Materials Science and Engineering, NTNU Norwegian University of Science and Technology, NO-7491, Trondheim, Norway.

sacrificial powder (procedure II) as described in Ref. 16. Sintering prosedure II was applied to investigate the effect of reducing loss of BaO during sintering. The materials were sintered at 1600 °C for 10 h using a heating rate of 600 °C/h. The samples denoted BZY10*, BZY20*, and BCZY27* were sintered by procedure II. The sacrificial powder consisted of BZY20 synthesized via solid state reaction from stoichiometric amounts of oxides at 1400 °C for 10 h and 10 wt% $BaCO_3$ (ACS Reagent, ≥99%, Sigma-Aldrich). The surface of the sintered specimens was polished with SiC papers and diamond suspensions down to 1 µm to obtain smooth surfaces.

2.2 Hydration of the ceramics

A dry reference state of the polished ceramics was achieved by heat treatment at 800 °C for 10 h in dry synthetic air (pH_2O < 10 Pa) to remove any traces of carbonates and water. Hydration of the materials was performed by passing wet gas with a constant gas flow over the dense samples in a tube furnace at temperatures ranging from 450 to 800 °C for 1 to 20 h. Humid air with a fixed water vapor pressure, pH_2O = 2700 Pa, was achieved by passing synthetic air through a saturated aqueous solution of potassium bromide (KBr). The heating and cooling rates were fixed to 300 and 400 °C/h, respectively. In addition, heat treatment of all the materials was performed at 500 °C in wet (10 h) followed by flow of dry synthetic air (2 and 10 h).

2.3 Characterization of the ceramics

The water uptake due to hydration was determined by comparing the mass of the same specimen in dried and hydrated state recorded with a balance (±0.0001 g). The proton content, $[OH_O^{\bullet}]$, was evaluated from the following relationship (eq. 1),

$$[OH_O^{\bullet}] = 2\frac{\Delta m}{m_0}\frac{M_{BZY}}{M_{H_2O}} \quad (1)$$

where m_0 is the mass of the dried sample, Δm is the mass uptake after hydration, M_{BZY} and M_{H2O} are the molecular weights of appropriate BZY and H_2O, respectively. The degree of hydration, $[OH_o]/[A]$, of the material was calculated dividing the proton content by acceptor dopant concentration, [A] = [Y]: $[Y]_{BZY10/BCZY27}$ = 0.1; $[Y]_{BZY20}$ = 0.2.

The density of the materials was measured by the Archimedes method using isopropanol at RT. All the sintered ceramics were characterized by X-ray powder diffraction (XRD) performed using a DaVinci2 diffractometer with $CuK_{\alpha 1}$ radiation. Diffraction patterns were recorded in the range 20° ≤ 2θ ≤ 60° with a scanning rate 0.35° min^{-1}. Rietveld refinement was carried out with the program TOPAS V4.1 using a cubic structure model $Pm\bar{3}m$ (no. 225) for all the materials. Initially, refinements were performed varying global parameters such as lattice parameters, peak shape parameters, background, phase fractions and sample displacement correction. Finally, fitting of the fractional occupancy and isotropic atomic displacement factors (ADFs) was also done.

The microstructure before and after Vickers indentation was characterized using a Hitachi S3400N scanning electron microscope (SEM). The samples were coated with gold. Grain size of sintered ceramics was estimated by the linear intercept method from SEM images of polished (1 µm diamond finish) and thermally etched (0.25 h, 1400–1450 °C) surfaces. The chemical composition of the phases was confirmed by Energy dispersive spectroscopy (EDS).

Mechanical properties of the polished ceramics were investigated by the Vickers micro-indentation technique (Leica VMHT MOT). The procedure and the conditions used are described in a recent report.[19]. Based on the previous investigation a load of 2 N was used in all the measurements. The distance between each indentation was more than 5 times the diagonal of the indent and load holding time was set to 10 s. The Vickers hardness of hydrated specimens was calculated applying geometrical measurements of indent size from SEM images using equation (2),[24]

$$H_v = 1.8544\frac{P}{d^2} \quad (2)$$

where P is the applied load (kg) and d is the mean length of diagonals (mm). The length of the cracks was measured geometrically and fracture toughness was estimated using the normalized Niihara's equation (3),[25]

$$K_{IC} = 9.518\left(\frac{c}{a}\right)^{-1.5}(H_v{}^{0.6})(a^{0.5}) \quad (3)$$

where K_{IC}, is the fracture toughness (MPa·$m^{1/2}$); a is 1/2 of indentation diagonal length (m); c is 1/2 of radial crack length (m) and H_v is the measured Vickers hardness (MPa). The choice of using Niihara's equation (eq. 3) was based on the criteria c/a>2.5.

3 Results

3.1 Unit cell parameters and microstructure of the sintered ceramics

Dense ceramics were obtained by both sintering procedures (I and II) in line with our previous report.[19] The density of all the ceramics were 94–95% relative to the theoretical density which was calculated from the lattice parameters determined by XRD. A linear dependence of the unit cell parameter with the Y-content was observed for the materials sintered by procedure II (Fig. 1a), while for the corresponding materials sintered by procedure I the unit cell was lower. The grain size was larger for the materials sintered by procedure II compared to the corresponding materials sintered by procedure I. The sintering procedure did not affect significantly the densification of pure $BaZrO_3$. The microstructure (density and grain size) and the unit cell parameters for all the materials are summarized in Table 1.

The BZY10 and BZY20 ceramics sintered by procedure I contained minor amounts of cubic Y_2O_3 according to the XRD

patterns, whereas the corresponding materials sintered by procedure II were phase pure according to XRD and SEM. The X-ray patterns of BZY10 and BZY10* are shown in Fig. 2. The amount of Y_2O_3 in the BZY10 and BZY20 sintered by procedure I, determined by XRD, is 1.5 and 2.0 wt%, respectively. Formation Y_2O_3 was avoided using procedure II, which show that the use of sacrificial powder reduce the loss of BaO during sintering. The absolute stoichiometry of the sintered materials could not be determined precisely since the loss of BaO is not known for any of the two sintering procedures.

3.2 Water uptake and chemical expansion due to hydration

The water (proton) uptake during hydration was measured by thermogravimetry using the dense pellets and the results are shown in Fig. 3. The data demonstrates that saturation was only obtained after close to 20 h hydration time (t) at 500 °C. The hydration of the bulk materials is therefore relatively slow at 500 °C and a gradient in the water content is expected eat times shorter than t ~ 20 h hydration time at 500 °C. The data in Fig. 3 implies that the maximum degree of hydration for the three different ceramics sintered by procedure I is ~0.3, whereas the degree of hydration is increased to ~0.5 for the same materials sintered by procedure II. The degree of hydration is clearly dependent on the overall stoichiometry of the main phase and strongly influenced by the loss of BaO during sintering.

The heat treatment in humid air resulted in a profound shift to smaller angles of the diffractograms up to 500 °C, whereas the shift was slightly lower for T > 500-550 °C. The variation in the unit cell parameter due to hydration of the three materials are illustrated in Fig. 4 and summarized in Table 1. An expansion of the lattice parameter is evident for all the ceramics exposed to humid air at 450 ≤ T ≤ 650 °C. The materials sintered by procedure I possess a maximum in chemical expansion at T ≈ 500–550 °C (Fig. 4a). The corresponding data for the materials sintered by procedure II and hydrated at 500 °C are shown in

Table 1. Hydration/dehydration time, unit cell parameter, Vickers hardness and fracture toughness of the materials sintered at 1600 °C in air before and after exposure to wet followed by dry synthetic air at 500 °C. The error in the cell parameters are $\pm 10^{-3}$.

Compound	Hydration time (h)	Dehydration time (μm)	Cubic cell parameter (Å)	Grain size (nm)	Vickers Hardness (H_v)	Fracture toughness ($MPa \cdot m^{1/2}$)
BZ	–	–	4.193	990±140	868±23	1.81±0.18
BZY10	–	–	4.198	240±10	895±19	1.86±0.05
	10	0	4.202	240±10	1005±29	2.43±0.07
	10	2	4.199	240±10	948±10	1.93±0.08
	10	10	4.198	240±10	910±14	1.88±0.09
BZY10*	–	–	4.207	520±40	742±7	1.58±0.13
	10	–	4.212	520±40	753±8	2.11±0.13
BZY20	–	–	4.215	640±30	801±20	1.79±0.08
	10	0	4.219	640±30	833±15	2.43±0.09
	10	2	4.216	640±30	808±10	1.88±0.11
	10	10	4.215	640±30	797±12	1.78±0.10
BZY20*	–	–	4.217	1100±50	675±10	1.49±0.11
	10	–	4.223	1100±50	701±6	2.18±0.14
BCZY27	–	–	4.249	280±40	858±21	1.65±0.11
	10	0	4.257	280±40	837±25	2.84±0.11
	10	2	4.251	280±40	834±13	1.71±0.06
	10	10	4.249	280±40	844±9	1.66±0.05
BCZY27*	–	–	4.250	690±80	734±23	1.46±0.03
	10	–	4.257	690±80	743±9	2.20±0.12

Journal of Materials Chemistry A

ARTICLE

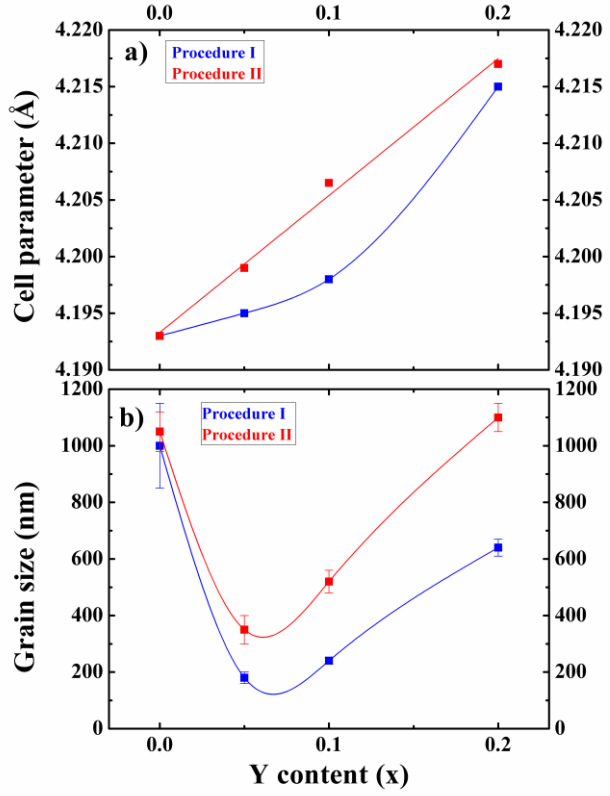

Fig. 1. The dependence of (a) cell parameter and (b) grain size on Y content, x, and sintering conditions of $BaZr_{1-x}Y_xO_{3-x/2}$ ceramics. Procedure I – sintering without sacrificial powder; procedure II – sintering with sacrificial powder (BZY20 and 10 wt% $BaCO_3$).

Fig. 4b. A systematic variation in the lattice parameters with hydration time can be observed. Finally, hydration for 10 h followed by drying for 10 h at 500 °C resulted in unit cell parameters equal to the ones observed for the initially dehydrated samples (Table 1).

The full-width-at-half-maximum (FWHM) of the (211) reflections for the dehydrated materials and hydrated ceramics at 500 °C for 10 h was compared. No significant difference in the FWHM was observed due to hydration except a minor increase for BZY10 after hydration.

3.3 Vickers micro-indentation of dry and hydrated/dehydrated ceramics

The microstructure of the materials was not altered by the hydration reaction. A representative SEM image of a typical Vickers indent in BZY10 after exposure to humid air at 500 °C for 10 h is shown in Fig. 5. A symmetrical square pyramid indent was observed for all materials both before and after thermal treatment in wet or dry atmosphere. Moreover, the indent pattern demonstrates that a single crack propagates from each of the four corners of the Vickers indent. The diagonal length of the indent and the crack length of the hydrated ceramics decreased relative to the characteristics of the indents in the initially dehydrated specimens. High resolution SEM images of the crack-ends in the pristine BZY10 and BCZY27 materials as well as the corresponding materials hydrated at 550 °C for 10 h are shown in Fig. 6a and 6b. The cracks propagated by an intergranular mode (along grain boundaries) in all the pristine materials both close to the indent and at the crack front. Interestingly, the cracks were observed to propagate along grain boundaries as well as through the grains (transgranular mode) after exposure to humid air (Fig. 6c and 6d). Moreover, fracture by intergranular mode was again observed in the samples hydrated and successively dehydrated at 500 °C.

The Vickers hardness of all the pristine materials measured using 2 N load is summarized in Table 1**.** The variation in the Vickers hardness of BZY10, BZY20, and BCZY27 ceramics due to hydration is summarized in Fig. 7a (and Table 1). The corresponding data for BZY10*, BZY20*, and BCZY27* is shown in Fig 7b. The Vickers hardness is affected by the hydration in most cases especially for BZY10 where hydration resulted in a significant increase in the hardness (Fig. 8a). A clear difference of the effect on the hardness with time can be seen at T < 500 °C and T > 500 °C indicating the influence of the degree and rate of hydration in the temperature range 450-650 °C. Notably, the Vickers hardness of the samples hydrated (10 h) and then dried (10 h) at 500 °C correspond well with the hardness of the pristine materials (Table 1).

The dependence of the fracture toughness of BZY10, BZY20, and BCZY27 on the heat treatment temperature in humid air is displayed in Fig. 8. The corresponding data for BZY10*, BZY20*, and BCZY27* is also included in the figure. The fracture toughness of the materials is strongly affected by the hydration and is increasing from 450 °C followed by a slight decrease at the highest temperatures investigated. Hydration of the oxygen vacancies at 450-650 °C therefore induces clearly a toughening of the BZY-ceramics. BZY10 and BZY10* with the smallest grains show the least profound increment in the fracture toughness (Fig. 8a). The fracture toughness was slightly reduced by increasing the hydration time from 1 to 10 h at *T* > 500 °C. A pronounced higher effect of hydration was observed after 1 h hydration time for the two highest temperatures. The fracture toughness of the ceramics exposed to wet (10 h) followed by dry air at 500 °C is summarized in

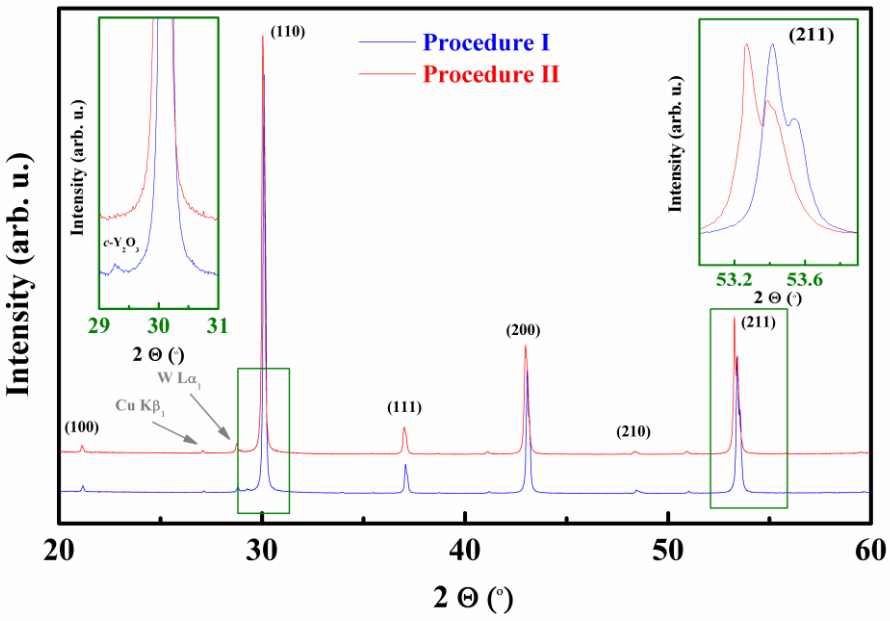

Fig. 2. XRD patterns of $BaZr_{0.9}Y_{0.1}O_{2.95}$ (BZY10) sintered without (procedure I) and with (procedure II) sacrificial powder. Insets: left - (110) and (111) diffraction peaks of cubic BZY10 and Y_2O_3, respectively; right – (211) diffraction peak of BZY10.

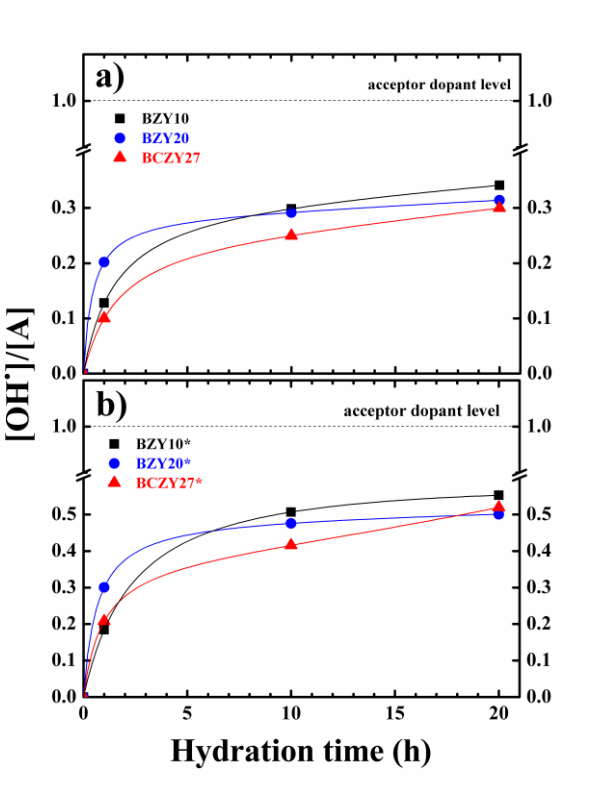

Fig. 3. The degree of hydration of $BaZr_{1-x}Y_xO_{3-x/2}$ and $BaCe_{0.2}Zr_{0.7}Y_{0.1}O_{2.95}$ ceramics, sintered by (a) procedure I and (b) procedure II, versus hydration time at 500 °C, pH_2O = 2700 Pa.

Table 1 and Fig. 9. Dehydration of the hydrated materials resulted in mechanical properties similar to the initial dry materials.

4 Discussion

4.1 Hardness and fracture toughness of pristine dry BZY-ceramics

The hardness of the pristine materials reported in this study is quite similar to the hardness reported for comparable oxide materials.[19, 26-33] Hardness of a material depends on the strength of the chemical bond and the Young's modulus and microstructural features such as grain size, porosity and surface roughness, and mechanically induced stress at the surface of materials after polishing.[34] A systematic variation in the Vickers hardness with regards to the grain size and Y-content in the pristine materials was observed (see Fig. 7) demonstrating that BZY10 with the smallest grain size possesses the highest hardness. The Vickers hardness of the ceramics sintered with sacrificial powder (procedure II) is considerably lower relative to the hardness of the materials sintered by procedure I (see Table 1). This is most likely related to the larger grain size of the latter and the absence of Y_2O_3 secondary phase in the materials sintered by procedure II. For the materials sintered by procedure II the hardness was not altered significantly by the hydration reaction (see Fig. 8). The hardness increased significantly by hydration only for BZY10, where both the hydration time and temperature were observed to influence on the hardness. This is also the material

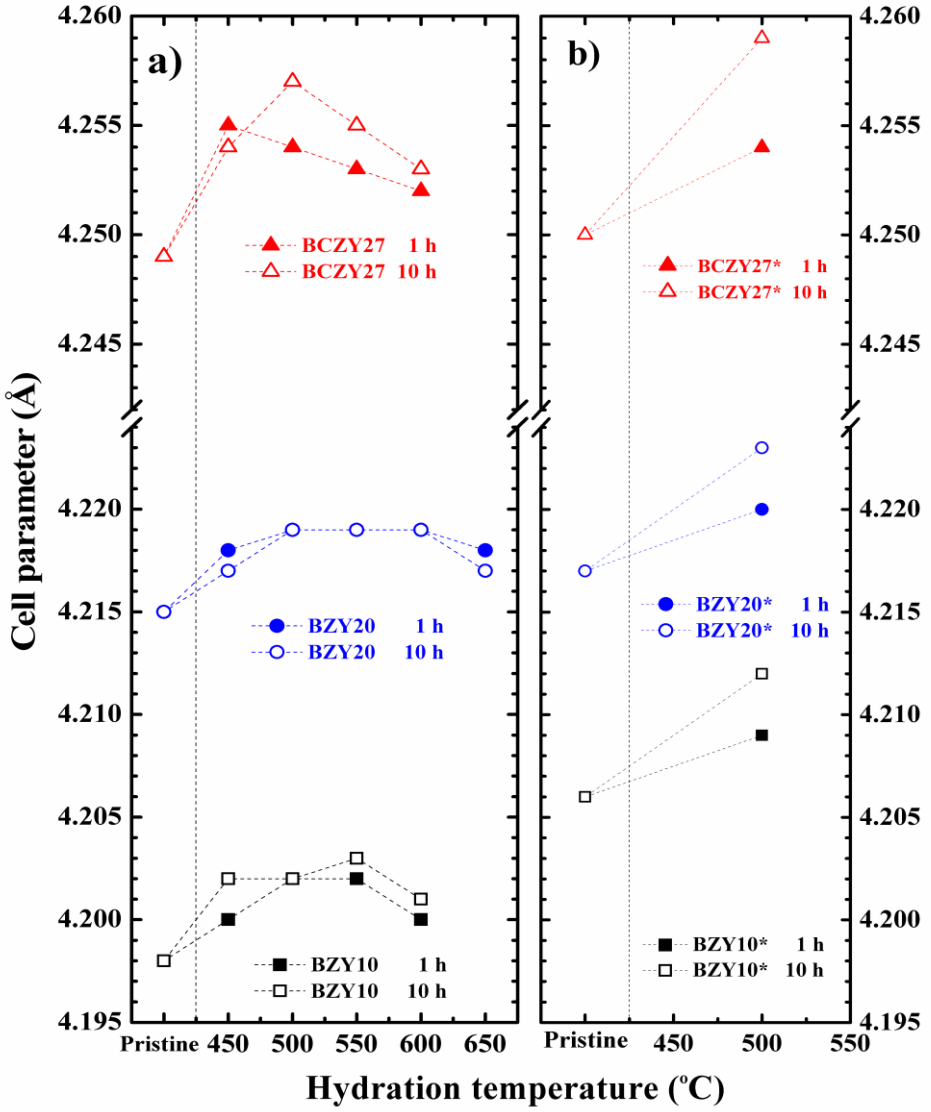

Fig. 4. The changes in cubic unit cell parameters of $BaZr_{1-x}Y_xO_{3-\delta}$ and $BaCe_{0.2}Zr_{0.7}Y_{0.1}O_{2.95}$ ceramics sintered by (a) procedure I and (b) procedure II, upon hydration at different temperatures, pH_2O = 2700 Pa. The errors in the cell parameters are $\pm 10^{-3}$.

with the smallest grain size.

Vickers indentation does not give an accurate absolute value for the fracture toughness, and one should be careful to discuss the variation of the estimated fracture toughness of the pristine materials with respect to composition and sintering procedure. The pristine materials have comparable estimated fracture toughness values. The most apparent trend is that sintering procedure II reduce the toughness, most likely related to a larger grain size and the absence of Y_2O_3 at the grain boundaries (in case of BZY10* and BZY20*).

4.2 Enhanced mechanical performance due to hydration of BZY-ceramics

The main objective of this work was to investigate the effect of hydration on the mechanical properties. The hydration reaction is known to be associated with lattice expansion.[22] The point defect reaction related to the hydration is defined as

$$H_2O(g) + v_O^{\bullet\bullet} + O_O^x \Leftrightarrow 2OH_O^{\bullet} \quad (4)$$

where $[v_O^{\bullet\bullet}]$, $[O_O^x]$ and $[OH_O^{\bullet}]$ are the concentrations of oxygen vacancies, oxygen on oxygen sites and protons (hydroxides) in the

Journal of Materials Chemistry A

ARTICLE

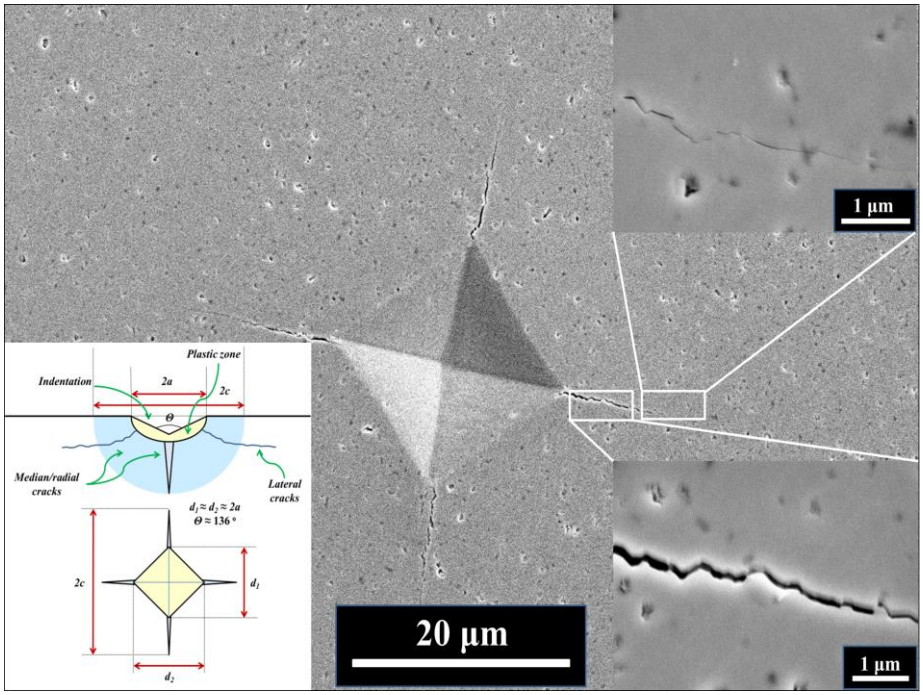

Fig. 5. SEM image of the indentation on the surface of BZY10 after heat treatment in humid synthetic air, pH_2O = 2700 Pa. Insets: left – indentation scheme; right – crack-start and crack-end.

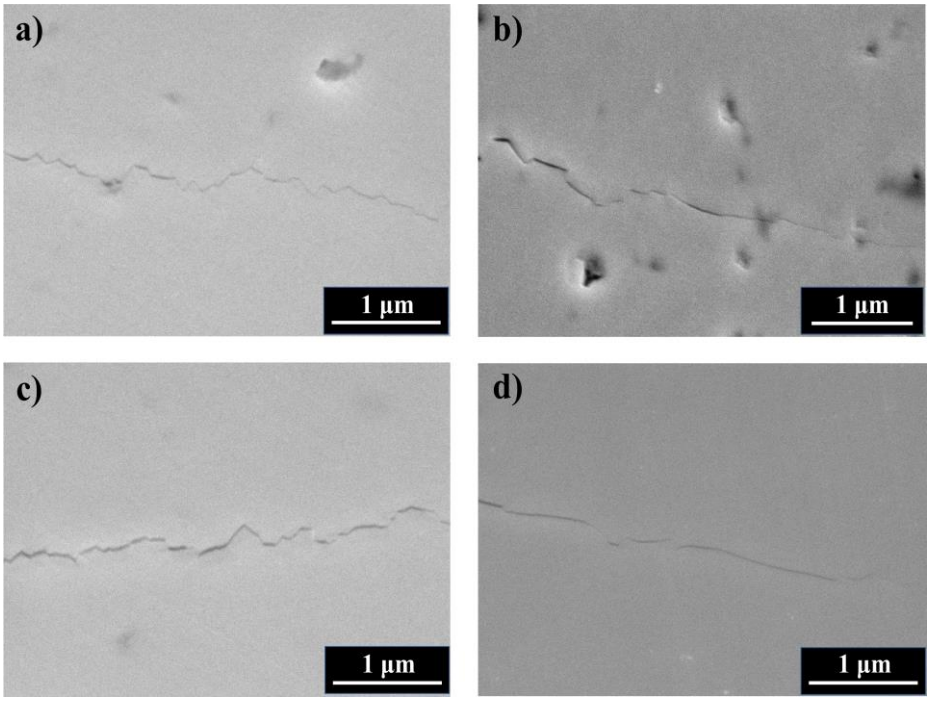

Fig. 6. SEM images of the front of the crack after indentation on the surface of the pristine (left column) and hydrated (right column) at 550 °C for 10 h, (a)-(b) BZY10 and (c)-(d) BCZY27 ceramics, pH_2O = 2700 Pa.

Journal of Materials Chemistry A

ARTICLE

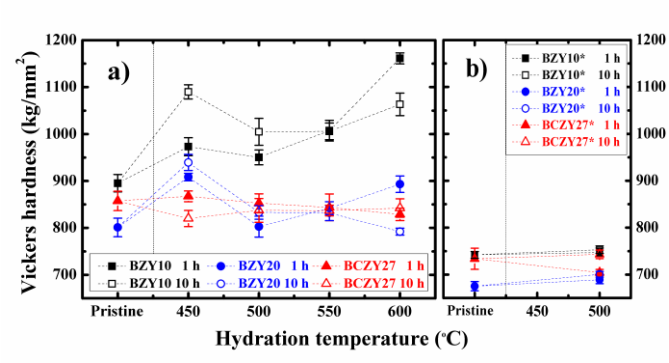

Fig. 7. The dependence of Vickers hardness on temperature and time for $BaZr_{1-x}Y_xO_{3-x/2}$ and $BaCe_{0.2}Zr_{0.7}Y_{0.1}O_{2.95}$ ceramics sintered by (a) procedure I and (b) procedure II under humid synthetic air, pH_2O = 2700 Pa.

lattice. The equilibrium constant (K) for the defect equilibrium (4) can be expressed as follows

$$K = \frac{\left[OH_O^{\bullet}\right]^2}{\left[V_O^{\bullet\bullet}\right]\left[O_O^{x}\right]p_{H_2O}} = \exp\left(-\frac{\Delta H_m}{RT} + \frac{\Delta S_m}{R}\right) \qquad (5)$$

where p_{H_2O} is the partial pressure of water. The enthalpy (ΔH_m) and entropy (ΔS_m) for reaction (4) have been determined for BZY as well as many other proton conducting oxides.[35] ΔH_m is exothermic while ΔS_m is negative, which means that the degree of hydration due to (4) increases with decreasing temperature until a certain concentration of $[OH_O^{\bullet}]$ becomes frozen in due to the slow dynamics (diffusion controlled) of the reaction. The reduction in the concentration of protons at elevated temperatures causes the characteristic maximum in the proton conductivity.[9]

Our initial hypothesis was that the kinetics of the hydration reaction (and dehydration) would strongly influence the mechanical properties observed by Vickers indentation. Four different conditions of the materials can be envisaged as defined in Fig. 10. First, the materials can be partially hydrated at relatively short hydration time inducing a gradient in $[OH_O^{\bullet}]$ which decrease rapidly from the surface to the bulk (state I). The vacancy concentration is inversely proportional to the proton content. Second, equilibration of reaction (4) will be obtained after long exposure time to the humid atmosphere resulting in a negligible gradient in the proton concentration as well as the oxygen vacancy concentration (state II). In this case the entire volume of the specimen is equilibrated with respect to reaction (4). Third, successive drying or dehydration of the materials will induce an opposite gradient in $[OH_O^{\bullet}]$ (state III). The last state IV is obtained after complete drying of the

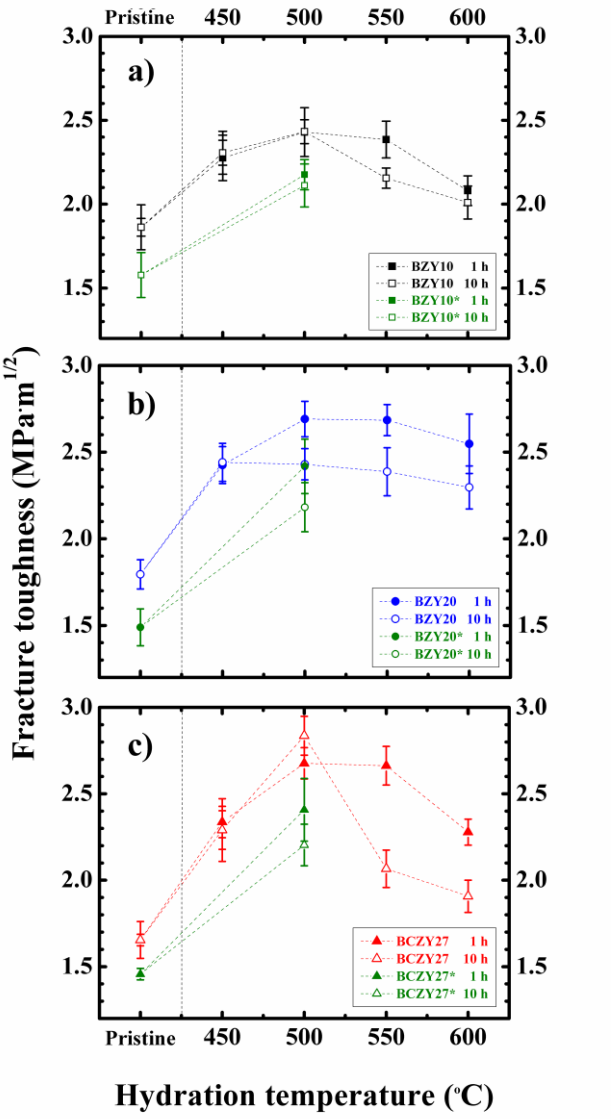

Fig. 8. The dependence of fracture toughness for $BaZr_{1-x}Y_xO_{3-x/2}$ (a), (b) and $BaCe_{0.2}Zr_{0.7}Y_{0.1}O_{2.95}$ ceramics (c) sintered by two different procedures on hydration temperature and time, pH_2O = 2700 Pa.

specimens, which correspond to close to zero concentration of protons and again no gradient in defect concentrations.

We had anticipated that transient states (State I and III) between the hydrated and the dry states would have the strongest effect on the mechanical properties due to the chemically induced compressive or tensile stress during respectively hydration and dehydration as illustrated in Fig. 10.

Compressive stress during hydration is caused by the chemical expansion due to hydration, while tensile stress during dehydration is due to the lattice contraction during dehydration.[22]

The strong influence of the hydration time on the fracture toughness (Fig. 8) is a solid indication of chemical induced stress in the materials during hydration. Above 500 °C the fracture toughness observed after 1 h was clearly higher than after 10 h hydration. At these temperatures the kinetics of the hydration reaction is faster than observed at 500 °C (Fig. 3) and one would expect that equilibrium was nearly reached after 10 hour reducing possible effects of gradients in the defect concentrations (state II, Fig. 10). However, after only 1 h of hydration a compressional stress at the surface is most likely (state I, Fig. 10). A compressional stress at the surface would lead to increased fracture strength, which would result in a higher fracture toughness as observed by the Vickers indentation.[36, 37]

The toughening of the ceramics goes through a maximum at 500-550 °C (Fig. 8). The reduction in the toughening above this temperature region is due to the reduced degree of hydration also reflected in the observed lattice constants (Fig 4). The reduced degree of hydration is expected based on the thermodynamics of reaction 4 where the negative entropy leads to reducing concentration of protons with increasing temperature. The toughening effect of hydration is therefore clearly proportional to the concentration of $[OH_O^{\bullet}]$.

The tenuously reduced fracture toughness nearly down to the pristine values after 2 h drying shows that it was not possible to fully dry the samples within this time frame (see Fig. 9). The fracture toughness values after short hydration/dehydration demonstrate that the mechanical properties are associated with the gradient in proton concentration as illustrated by states I and III (Fig. 10).

The most striking effect of the hydration of the oxide ceramics studied here is the transformation from intergranular to transgranular mode of the radial cracks propagating from the corners of the Vickers indents (Fig. 6). The change in fracture mode and shorter crack length and consequently increased estimated fracture toughness were observed for all the materials. Interestingly, the effect was demonstrated to be reversible and the intergranular mode was recovered after complete dehydration of the materials. The change in fracture mode gives strong evidence that the hydration of these proton conducting materials strengthen the grain boundaries resulting in transgranular fracture of the materials. The role of the grain boundaries in $BaZrO_3$-based materials have been heavily debated due to the high resistivity in relation to the proton conductivity. A corresponding effect of hydration on the hardness was not observed although an increased hardness due to hydration was observed for BZY10.

The strengthening of the grain boundaries due to the hydration reactions needs further attention. Reaction (4) is reported to be exothermic,[9] showing that new bonds are formed when the oxygen vacancies are filled with hydroxide ions. We therefore propose that the increased strength of the grain boundary is caused by filling of oxygen vacancies located at the grain boundaries strengthening the chemical bonding at the grain boundaries resulting in a toughening of the materials.

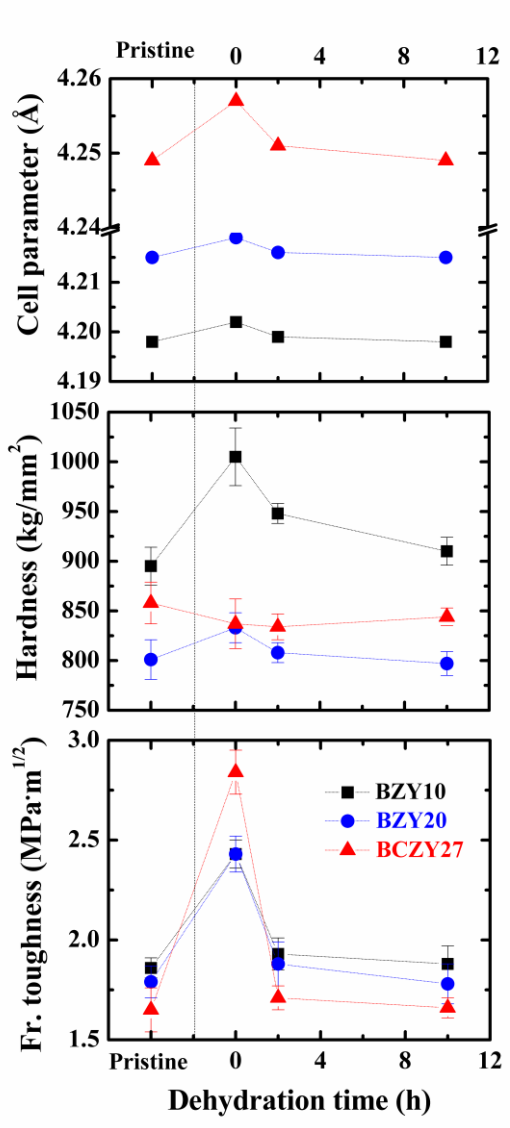

Fig. 9. The dependence of cell parameter and mechanical properties for $BaZr_{1-x}Y_xO_{3-x/2}$ and $BaCe_{0.2}Zr_{0.7}Y_{0.1}O_{2.95}$ ceramics on dehydration time, pH_2O = 2700 Pa. The samples were hydrated at 500 °C for 10 h prior to dehydration (t = 0).

The present results demonstrate that the challenges with low mechanical performance of proton-conducting oxides[9] is most likely not related to chemically induced microcracking due to reaction (4) during either hydration or dehydration.

The current data on mechanical performance of Y-doped $BaZrO_3$ is a clear evidence that these ceramics are robust electrolytes in steam environment. The hydration/dehydration of the ceramics is a reversible process, which can be controlled, and reaction (4) does not induce reduced mechanical stability and microcracking in the materials. Finally, the present work have shown that gradients in the

humidification level did not show evidence of reduction in the mechanical performance. This is also promising with respect to the long-term stability of fuel cells or electrolyzers based on $BaZrO_3$.

4.3 Chemical expansion due to hydration in BZY-ceramics

The data shown in Fig. 4 demonstrates that hydration of ceramics results in an expansion of the lattice in agreements with previous reports.[22] BZY containing different Y contents exhibits similar change in lattice constant and the magnitude does not seem to increase with the increasing Y content. BCZY27 shows the most profound change in the cell parameter. This phenomenon could be explained by the incorporation of larger Ce^{4+} cations on the B-site in the perovskite lattice. Notably, increased hydration (procedure II) increases the overall change of the cell parameters upon hydration at 500 °C. The absence of new reflections and the similarity of FWHM before and after hydration disregard any phase change during hydration.

The hydration of oxygen vacancies results in expanded cell parameters to a maximum at a certain temperature (see Fig. 5). Above this temperature the cell parameters decreased. Since $\Delta S_m < 0$ for reaction (4), the equilibrium is shifted to the left and the proton concentration as well as chemical expansion is reduced at higher temperatures (see Fig. 4a). Reaction (4) is a reversible reaction and the unit cell parameter of the pristine materials could be obtained after dehydration (see Table 1 and Fig. 9).

The calculated chemical strain and expansion of oxide materials due to hydration reaction (4) at 500 °C are presented in Table 2. The chemical strain (ε_C) is calculated from the unit cell parameters of the hydrolyzed and dry materials (Table 1) and are shown in Table 2. The normalized chemical strain, $\varepsilon_C/\Delta y_H$, and the chemical expansion coefficient (β_{hydr}) are calculated from Δy_H measured by the thermogravimetrical analysis.[22] The reported chemical expansion of the materials is within the same order of magnitude for all the materials, varying between 0.014 and 0.063, which is in a good agreement with literature data on hydration for similar compositions.[38] The chemical expansion caused by hydration of perovskite oxide materials is clearly not constant. Apparently, our results show that the sintering conditions (procedure II) or increased Y content in BZ reduces the normalized chemical strain due to hydration.

4.4 Chemical aspects of hydration of BZY-ceramics

The uptake of water should reach a constant value at equilibrium for reaction (4) at a constant partial pressure of water and constant temperature. The water (proton) uptake in the BZY ceramics measured gravimetrically is represented in Fig. 3.

The equilibrium concentration of protons was clearly dependent on the sintering procedure and was found to be higher for the materials sintered by procedure II. This means that either the concentration of oxygen vacancies or the thermodynamics of reaction (4) are influenced by the sintering procedure. In the following, we discuss these two scenarios.

The concentration of oxygen vacancies in dry (dehydrated) BZ is controlled by acceptor (Y) doping as described by reaction (6)

$$2Zr_{Zr}^{x} + O_O^x + Y_2O_3(s) \Leftrightarrow 2Y_{Zr}^{'} + v_O^{\bullet\bullet} + 2ZrO_2(s) \qquad (6)$$

However, if the concentration of other point defects becomes significant the assumption that $[v_O^{\bullet\bullet}] = [Y_{Zr}^{/}]$ in dry BZY does not hold.

When the samples are sintered without sacrificial powder (procedure I), the loss of BaO becomes more pronounced. The change in phase content and microstructure of BZY due to the loss of BaO have been studied at $T \geq 1600$ °C.[32] Two different reactions can be proposed due to loss of BaO.[2, 32] Firstly, the loss of BaO(g) can be compensated by precipitation of Y_2O_3 as expressed by equation (7)[32, 39]

$$BaZr_{0.9}Y_{0.1}O_{2.95}(s) \Leftrightarrow \alpha BaO(g) + \frac{\beta}{2}Y_2O_3(s) + Ba_{1-\alpha}Zr_{0.9}Y_{0.1-\beta}O_{2.95-\delta}(s) \qquad (7)$$

We have observed the presence of Y_2O_3 in BZY10 and BZY20 (see Fig. 2). The formation of Y_2O_3 is accompanied by a reduction in the Y-content and thereby a reduction in the unit cell of BZY.[32, 40] On the other hand, when the samples were sintered with sacrificial powder (procedure II) no cubic Y_2O_3 could be detected by XRD. The high BaO activity in the sacrificial powder suppressed the loss of BaO and thereby also suppressing the formation of Y_2O_3.

A second possible effect of loss of BaO is transfer of Y to the A-site in the perovskite lattice according to reaction (8)[32]

$$2Ba_{Ba}^{x} + v_O^{\bullet\bullet} + Y_2O_3(s) \Leftrightarrow 2Y_{Ba}^{\bullet} + O_O^x + 2BaO(s) \qquad (8)$$

Table 2. Chemical strain (ε_C), proton concentration (Δy_H) normalized chemical strain (ε_C /Δy_H) and chemical expansion coefficient (β_{hydr}) after hydration of proton-conducting ceramic oxides. $\varepsilon_C=(a-a_o)/a_o$ where a and a_o is the unit cell of the hydrated and dehydrated samples.

Material	ε_C	Δy_H	$\varepsilon_C/\Delta y_H$	β_{hydr} ($3\varepsilon_C/\Delta y_H$)
$BaZr_{0.9}Y_{0.1}O_{2.95}$ (BZY10)	0.0012	0.034	0.035	0.105
$BaZr_{0.9}Y_{0.1}O_{2.95}$* (BZY10*)	0.0014	0.055	0.025	0.075
$BaZr_{0.8}Y_{0.2}O_{2.9}$ (BZY20)	0.0009	0.063	0.014	0.042
$BaZr_{0.8}Y_{0.2}O_{2.9}$* (BZY20*)	0.0014	0.1	0.014	0.042
$BaCe_{0.2}Zr_{0.7}Y_{0.1}O_{2.95}$ (BCZY27)	0.0019	0.03	0.063	0.189
$BaCe_{0.2}Zr_{0.7}Y_{0.1}O_{2.95}$* (BCZY27*)	0.0021	0.052	0.04	0.12

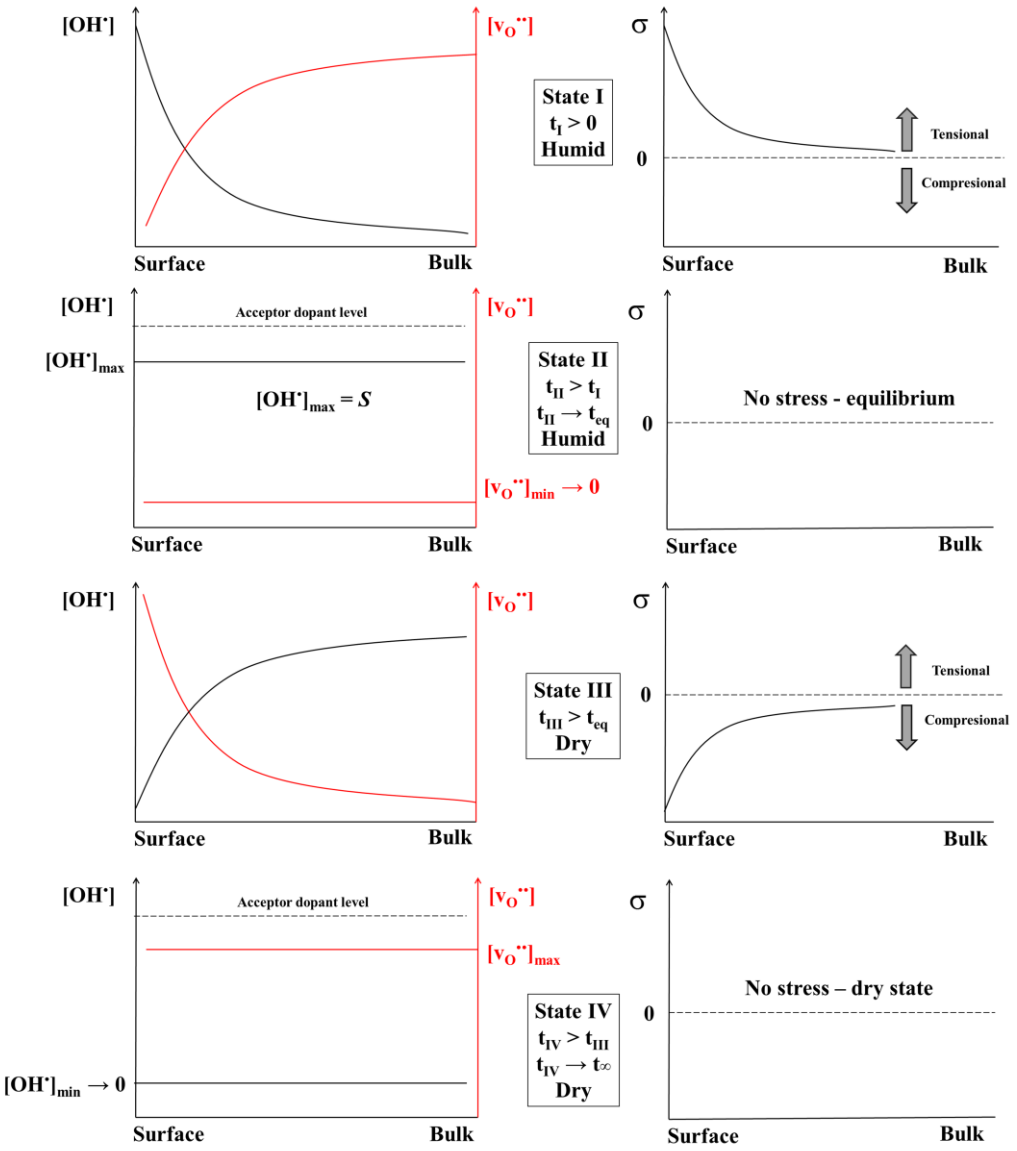

Fig. 10. A schematic representation of three possible states in the ceramics on hydration/dehydration.

Reaction (8) has the major consequence that the concentration of oxygen vacancies in dry BZY are no longer equal to twice the concentration of Y. Y on Ba-site is expected to cause a shrinkage of the lattice due to the size difference of the cations[41] as Fig. 1 indicates. However, the reduction in the Y-content on the Zr-site will also lead to a reduction of the lattice unit cell. Hence, evidence for reaction (8) cannot be provided simply by an analysis of the unit cell only.

Both reaction (7) and (8) will reduce the acceptor doping level with the consequence that the concentration of oxygen vacancies will be reduced. While reaction (7) is verified by the presence of Y_2O_3, experimental evidence of Y on Ba size is challenging since reduction in the unit cell of BZY is expected for both reactions. A linear behavior of cell parameter versus Y content was observed for samples sintered by procedure II (Fig. 3), supporting that Y is mainly at the B-site in the perovskite in these samples.[32]

A special attention was given to consider the saturation limit, *S*, which determines the effective concentration of protonic defects (water saturation limit) in the material.[9] Ideally, the equilibrium concentration should be equal to the acceptor dopant concentration, *S* = [Y] at high partial pressure of water and low temperature. However, *S*/[Y] < 1 and is often found difficult to reproduce.[9] The concentration of protons normalized with respect to the total dopant level, [Y], demonstrates that the degree of hydration approaches 0.3 and 0.5 at 500 °C dependent on the sintering procedure, see Fig. 3. According to thermodynamics, the equilibrium degree of hydration at 500 °C for BZY10 and BZY20 are ~0.7 and 0.6, respectively (pH_2O = 2300 Pa).[42] The lower degree of hydration observed here is inferred to be a consequence of the influence

of point defect equilibria such as (7) or (8). The degree of hydration is remarkably similar for the two different sintering procedures, supporting the hypothesis that loss of BaO has a huge influence on the phase content and the concentration of point defects in BZY.

Finally, the transient stress at the surface during hydration and dehydration will also influence on the kinetics of reaction (4). The increased pressure due to the compression at the surface (Fig. 10) will give an apparent shift of the equilibrium to the right since $d(G)/dp = V$ and $\Delta V > 0$.

Conclusions

Dense and phase pure doped barium zirconate ceramics, $BaZr_{1-x}Y_xO_{3-\delta}$ (x = 0.1 and 0.2) and $BaCe_{0.2}Zr_{0.7}Y_{0.1}O_{2.95}$, were successfully prepared by solid state sintering of powders prepared by spray pyrolysis. The degree of hydration of the ceramics was determined by thermogravimetrical analysis, and the chemical strain was determined combining these data with the unit cell parameters of dry and hydrated materials. The change in mechanical properties of the materials due to hydration was investigated by Vickers micro-indentation. An enhanced fracture toughness of the materials was observed due to the hydration reaction at elevated temperatures. The fracture mode of the materials changed from transgranular to intergranular by hydration. The properties of the pristine dry materials were reestablished by dehydration of the materials demonstrating that the hydration/dehydration reactions are reversible. Based on the present findings the effect of hydration on the mechanical performance of BZY-materials is discussed in relation to the use of these materials as electrolytes in intermediate temperature protonic ceramic fuel cells and electrolyzers.

Acknowledgements

Financial support from The Research Council of Norway under the program NANO2021 to the project (Number 228355) "Functional oxides for clean energy technologies: fuel cells, gas separation membranes and electrolysers" (FOXCET) conducted by SINTEF Materials and Chemistry, University of Oslo and NTNU The Norwegian University of Science and Technology in Trondheim, is gratefully acknowledged.

References

1 P. Babilo and S. M. Haile, *J. Am. Ceram. Soc.*, 2005, **88**, 2362.

2 P. Babilo, T. Uda and S. M. Haile, *J. Mater. Res.*, 2007, **22**, 1322.

3 Y. Yamazaki, R. Hernandez-Sanchez and S. M. Haile, *Chem. Mater.*, 2009, **21**, 2755.

4 J. Tong, D. Clark, M. Hoban and R. O'Hayre, *Solid State Ionics*, 2010, **181**, 496.

5 D. Pergolesi, E. Fabbri, A. D'Epifanio, E. Di Bartolomeo, A. Tebano, S. Sanna, S. Licoccia, G. Balestrino and E. Traversa, *Nat. Mater.*, 2010, **9**, 846.

6 E. C. C. d. Souza and R. Muccillo, *Mater. Res.*, 2010, **13**, 385.

7 C. Duan, J. Tong, M. Shang, S. Nikodemski, M. Sanders, S. Ricote, A. Almansoori and R. O'Hayre, *Science*, 2015, **349**, 1321.

8 L. Malavasi, C. A. J. Fisher and M. S. Islam, *Chem. Soc. Rev.*, 2010, **39**, 4370.

9 K. D. Kreuer, *Ann. Rev. Mater. Res.*, 2003, **33**, 333.

10 K. D. Kreuer, *Solid State Ionics*, 1999, **125**, 285.

11 H. Iwahara, T. Yajima, T. Hibino, K. Ozaki and H. Suzuki, *Solid State Ionics*, 1993, **61**, 65.

12 T. Schober and H. G. Bohn, *Solid State Ionics*, 2000, **127**, 351.

13 H. Iwahara, H. Uchida, K. Ono and K. Ogaki, *J. Electrochem. Soc.*, 1988, **135**, 529.

14 B. Zhu, X. Liu and T. Schober, *Electrochem. Comm.*, 2004, **6**, 378.

15 T. Shimura, H. Tanaka, H. Matsumoto and T. Yogo, *Solid State Ionics*, 2005, **176**, 2945.

16 S. Gopalan and A. V. Virkar, *J. Electrochem. Soc.*, 1993, **140**, 1060.

17 K. H. Ryu and S. M. Haile, *Solid State Ionics*, 1999, **125**, 355.

18 D. Medvedev, J. Lyagaeva, S. Plaksin, A. Demin and P. Tsiakaras, *J. Pow. Sour.*, 2015, **273**, 716.

19 R. Sažinas, C. Bernuy-López, M.-A. Einarsrud and T. Grande, *J. Am. Ceram.Soc.*, 2016, 1.

20 A. Braun, A. Ovalle, V. Pomjakushin, A. Cervellino, S. Erat, W. C. Stolte and T. Graule, *App. Phys. Lett.*, 2009, **95**, 224103.

21 C. Hiraiwa, D. Han, A. Kuramitsu, A. Kuwabara, H. Takeuchi, M. Majima and T. Uda, *J. Am. Ceram. Soc.*, 2013, **96**, 879.

22 A. K. Eriksson Andersson, S. M. Selbach, C. S. Knee and T. Grande, *J. Am. Ceram. Soc.*, 2014, **97**, 2654.

23 A. K. Eriksson Andersson, S. M. Selbach, T. Grande and C. S. Knee, *Dalton Transactions*, 2015, **44**, 10834.

24 *ASTM E384 Standard test method for microhardness of materials*, 1984.

25 K. Niihara, R. Morena and D. P. H. Hasselman, *J. Mater. Sci. Lett.*, 1982, **1**, 13.

26 S. Yamanaka, M. Fujikane, T. Hamaguchi, H. Muta, T. Oyama, T. Matsuda, S.-i. Kobayashi and K. Kurosaki, *J. All. Comp.*, 2003, **359**, 109.

27 R. Vassen, X. Cao, F. Tietz, D. Basu and D. Stöver, *J. Am. Ceram. Soc.*, 2000, **83**, 2023.

28 T. Maekawa, K. Kurosaki and S. Yamanaka, *J. All. and Comp.*, 2006, **407**, 44.

29 G. Panomsuwan, O. Takai and N. Saito, *Physica Status Solidi (a)*, 2013, **210**, 311.

30 W. Ma, D. E. Mack, R. Vaßen and D. Stöver, *J. Am. Ceram. Soc.*, 2008, **91**, 2630.

31 D. Hassan, S. Janes and R. Clasen, *J. Eur. Ceram. Soc.*, 2003, **23**, 221.

32 Y. Yamazaki, C.-K. Yang and S. M. Haile, *Scripta Materialia*, 2011, **65**, 102.

33 T. Maekawa, K. Kurosaki, H. Muta, M. Uno, S. Yamanaka, T. Matsuda and S. Kobayashi, *Advances in Electronic and Electrochemical Ceramics: Proceedings of the 107th Annual Meeting of The American Ceramic Society,* Thermophysical Properties of Perovskite Type Alkaline Earth Hafnates, Ceramic Transactions, Baltimore, Maryland, USA, 2005.
34 I. J. McColm, *Ceramic Hardness*, Plenum Press, New York, 1990.
35 T. Norby and Y. Larring, *Current Opinion in Solid State and Materials Science*, 1997, **2**, 593.
36 G. R. Anstis, P. Chantikul, B. R. Lawn and D. B. Marshall, *Journal of the American Ceramic Society*, 1981, **64**, 533.
37 B. Lawn, *Fracture of Brittle Solids*, 2nd., Cambridge University Press, New York, 1993.
38 E. Jedvik, A. Lindman, M. Þ. Benediktsson and G. Wahnström, *Solid State Ionics*, 2015, **275**, 2.
39 Y. Yamazaki, R. Hernandez-Sanchez and S. M. Haile, *J. Mater. Chem.*, 2010, **20**, 8158.
40 M. D. Goncalves, P. S. Maram, R. Muccillo and A. Navrotsky, *J. Mater. Chem. A*, 2014, **2**, 17840.
41 R. D. Shannon, *Acta Crystallographica Section A*, 1976, **32**, 751.
42 K. D. Kreuer, S. Adams, W. Munch, A. Fuchs, U. Klock and J. Maier, *Solid State Ionics*, 2001, **145**, 295.